Shear heating reconciles thermal models with the metamorphic rock record of subduction

Matthew J. Kohn[a,1], Adrian E. Castro[b], Buchanan C. Kerswell[a], César R. Ranero[c,d], and Frank S. Spear[b]

[a]Department of Geosciences, Boise State University, Boise, ID 83725; [b]Department of Earth and Environmental Sciences, Rensselaer Polytechnic Institute, Troy, NY 12180; [c]Instituto de Ciencias del Mar, Spanish National Research Council, 08003 Barcelona, Spain; and [d]Institució Catalana de Recerca i Estudis Avançats, 08010 Barcelona, Spain

Edited by Peter B. Kelemen, Lamont-Doherty Earth Observatory, Palisades, NY, and approved October 4, 2018 (received for review June 14, 2018)

Some commonly referenced thermal-mechanical models of current subduction zones imply temperatures that are 100–500 °C colder at 30–80-km depth than pressure–temperature conditions determined thermobarometrically from exhumed metamorphic rocks. Accurately inferring subduction zone thermal structure, whether from models or rocks, is crucial for predicting metamorphic reactions and associated fluid release, subarc melting conditions, rheologies, and fault-slip phenomena. Here, we compile surface heat flow data from subduction zones worldwide and show that values are higher than can be explained for a frictionless subduction interface often assumed for modeling. An additional heat source—likely shear heating—is required to explain these forearc heat flow values. A friction coefficient of at least 0.03 and possibly as high as 0.1 in some cases explains these data, and we recommend a provisional average value of 0.05 ± 0.015 for modeling. Even small coefficients of friction can contribute several hundred degrees of heating at depths of 30–80 km. Adding such shear stresses to thermal models quantitatively reproduces the pressure–temperature conditions recorded by exhumed metamorphic rocks. Comparatively higher temperatures generally drive rock dehydration and densification, so, at a given depth, hotter rocks are denser than colder rocks, and harder to exhume through buoyancy mechanisms. Consequently—conversely to previous proposals—exhumed metamorphic rocks might overrepresent old-cold subduction where rocks at the slab interface are wetter and more buoyant than in young-hot subduction zones.

subduction | heat flow | thermal modeling | metamorphism | P–T paths

Determining the pressure–temperature (P–T) conditions of subduction zone metamorphism is key for understanding rock rheology, fluid-mass transfer and geochemical cycling of carbon, trace elements, and other chemical species between Earth's crust and mantle (e.g., refs. 1–3), genesis and chemistry of arc volcanoes (e.g., ref. 4), origin of shallow interplate seismicity (e.g., refs. 5–7), and H_2O release vs. storage in the mantle (e.g., refs. 8–10). Interpretations of these processes all depend strongly on thermal structure, yet at depths of 30–80 km, a 100–500 °C discrepancy occurs between many commonly cited, frictionless thermal models (11) and P–T conditions of subduction zone metamorphic rocks, as determined either from metamorphic facies (12, 13) or from thermobarometry (14–16). In this context, we make several comparisons to the most recent and comprehensive data compilation for rocks (16), using the term "PD15" to refer to the reported dataset and average geotherm. As shown previously (16), bias to the calculated P–T conditions through postpeak processes (transfer to hanging wall, residence times, isothermal exhumation, etc.) does not likely explain model-data discrepancies because prograde P–T paths show the same P–T distribution as thermobarometry. Rather, many numerical models predict slab-top geotherms that are <5 °C/km and enter a region of P–T space that metamorphic petrologists sometimes denote as the "forbidden zone" (17). No known rocks up to 4 GPa record such cold P–T conditions (14, 15).

Explaining the large temperature discrepancy between rocks and models could reveal either omission or underestimation of possible heat sources in models (16), or bias in the exhumation of subduction zone metamorphic rocks (10). Indeed, it was argued recently that all rocks exhumed from subduction zones reflect only warm subduction conditions (10), for example from subduction of anomalously young crust or from subduction initiation. In fact, dehydration forms dense garnet and pyroxene, so warmer and comparatively drier rocks from the slab interface should be denser (14, 18) and possibly more difficult to exhume than cooler, wetter rocks. Nonetheless, if widely accepted cold models (11) are correct, exhumed rocks provide few examples of P–T conditions predicted by these models.

To reassess temperatures along the subduction interface, we evaluated constraints on shear heating derived from global heat flow datasets and site-specific studies (see *SI Appendix* for sources). We then modeled the slab-top thermal structure using a simple but highly flexible analytical model (19, 20) that accounts for variations in the magnitudes of shear heating, thermal weakening, and other key subduction parameters (*Methods* and *SI Appendix*). We emphasize shear heating because it is a large potential contributor to slab-top temperature increases: Heat sources from reactions, fluid flow, radioactive heating, and convection have been estimated to be 2–10 times smaller (e.g., see ref. 21). More recent work (22, 23) has shown that fluid flow along the top of the subducting slab may reduce temperatures by up to ∼100 °C, which is comparable in magnitude to the effects of the lowest proposed coefficients of friction. Insofar as shear heating could theoretically increase slab-top geotherms by several hundred degrees Celsius (13, 21, 24), quantifying typical coefficients of friction and their thermal consequences is crucial to the reliability of any petrologic or geochemical interpretations.

Significance

Thermal structure controls numerous aspects of subduction zone metamorphism, rheology, and melting. Many thermal models assume small or negligible coefficients of friction and underpredict pressure–temperature (P–T) conditions recorded by subduction zone metamorphic rocks by hundreds of degrees Celsius. Adding shear heating to thermal models simultaneously reproduces surface heat flow and the P–T conditions of exhumed metamorphic rocks. Hot dry rocks are denser than cold wet rocks, so rocks from young-hot subduction systems are denser and harder to exhume through buoyancy. Thus, the metamorphic record may underrepresent hot-young subduction and overrepresent old-cold subduction.

Author contributions: M.J.K., B.C.K., C.R.R., and F.S.S. designed research; M.J.K., A.E.C., B.C.K., and C.R.R. performed research; M.J.K., A.E.C., and F.S.S. analyzed data; and M.J.K., A.E.C., C.R.R., and F.S.S. wrote the paper.

The authors declare no conflict of interest.

This article is a PNAS Direct Submission.

[1]To whom correspondence should be addressed. Email: mattkohn@boisestate.edu.

This article contains supporting information online at www.pnas.org/lookup/suppl/doi:10.1073/pnas.1809962115/-/DCSupplemental.

Published online October 29, 2018.

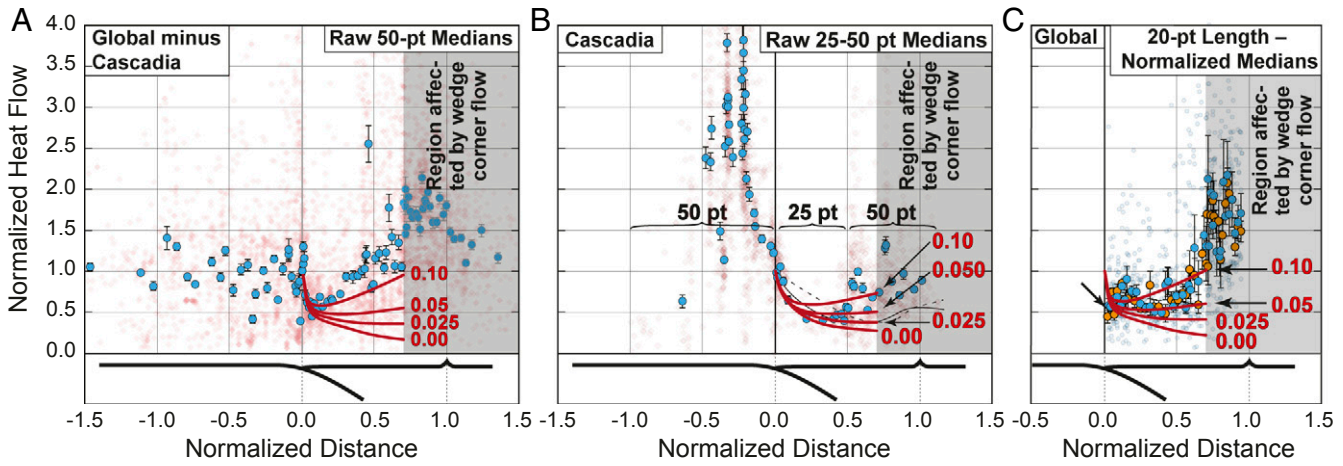

Fig. 1. Heat flow data (39) normalized to expected heat flow of incoming plate (25) vs. distance normalized to arc–trench distance. Model curves are labeled with assumed apparent coefficients of friction (μ*). Large dots with error bars are medians of binned data and their errors. Gray regions are affected by corner flow and are not considered in this study. (*A*) Raw data excluding Cascadia. Models are calculated using analytical approach of refs. 19 and 20, and assume global average modern subduction parameters: plate age = 50 Ma, convergence rate = 6 cm/y, subducting plate geometry = central Chile, thickness of crust in overriding plate = 20 km. About 6% of data fall above upper heat flow limit of 4.0. (*B*) Raw data for Cascadia. Models use average Cascadia subduction parameters: plate age = 8.5 Ma, convergence rate = 3.5 cm/y, subducting plate geometry = central Cascadia, thickness of crust in overriding plate = 35 km. About 33% of data fall above upper heat flow limit of 4.0. Thin solid line is from ref. 31; thin dashed line is from refs. 32 and 33. (*C*) All data between normalized distances of 0.02 and 1.0 for well-sampled subduction zones, randomly sampled in proportion to trench length. Arrow indicates region of anomalously low heat flow. Orange and blue medians show two random samples of the same data. Models use global average subduction parameters. About 5% of data fall above upper heat flow limit of 4.0.

As a complement to the global heat flow database, we also compiled estimates of the coefficient of friction in specific subduction zones. Last, we calculated densities for typical subducted rocks along three representative cold, intermediate, and hot P–T trajectories to identify whether cold vs. hot subduction might preferentially induce exhumation of rocks through buoyancy (*Methods* and *SI Appendix*).

Our overall intent is to integrate disparate models and observations—many made by others—to evaluate whether the exhumed metamorphic rock record reflects typical vs. atypical metamorphic P–T conditions expected in modern subduction environments. In this context, we hypothesize that integration of rock P–T conditions, geophysical observations of heat flow and rock strength, and thermal modeling reconcile thermal models with petrologic observations. We emphasize temperatures along the subduction interface (the boundary between the subducting slab and overlying plate) because it is thought to represent the region of maximum geochemical exchange, and to be the source of exhumed metamorphic rocks. We refer to the temperature distribution along this interface as the slab-top geotherm.

Context of Thermal Models and the Petrologic Record

Numerous studies have investigated key components of subduction zones that must be mutually integrated to evaluate rock vs. model P–T conditions. These include compilations of heat flow and estimated coefficients of friction; compilations of the peak P–T conditions of exhumed, subduction zone metamorphic rocks; calculations of rock density; experimental determination of rock strengths; and numerical and analytical thermal models of subduction zones. Much previous work addresses these topics. Our contribution is to expand and update the global heat flow dataset across current subduction systems compared with ref. 25, which provides constraints on realistic coefficients of friction; to calculate subduction zone thermal structure and rock densities along specified P–T paths using parameters that we argue more accurately represent typical thermal conditions along the top of the slab; and to critically review previous interpretations in the context of revised coefficients of friction.

Heat Flow and Friction. Heat flow measurements are typically unevenly distributed (*SI Appendix*, Fig. S1) and scattered (e.g., Fig. 1), so many studies focus on specific subduction zones with large numbers of measurements (see *SI Appendix* for data sources; Fig. 2). This approach elucidates some processes well, but also emphasizes a few subduction zones to the exclusion of others. Frictional heating is commonly calculated from a friction coefficient, which is multiplied by normal stress to determine shear stress. Intrinsic (μ) vs. apparent (μ*) coefficients of friction are determined from mechanical experiments on rocks vs. geophysical data (e.g., heat flow). μ* is lower than μ because other factors reduce shear strength, such as high pore fluid pressure or rapid shear rate.

P–T Compilations. For comparison with models, identification of typical P–T distributions from exhumed subduction zone rocks has been based on metamorphic facies (12, 13) (see also reviews of refs. 26 and 27 and recent work of ref. 28) and thermobarometry (14–16). Quantitative P–T conditions fall toward the hotter side of the fields that delimit blueschist and eclogite facies (Fig. 3). For example, the PD15 dataset shows that P–T conditions for blueschist-facies rocks are on average ∼100 °C higher than the midpoint of the blueschist-facies field (Fig. 3).

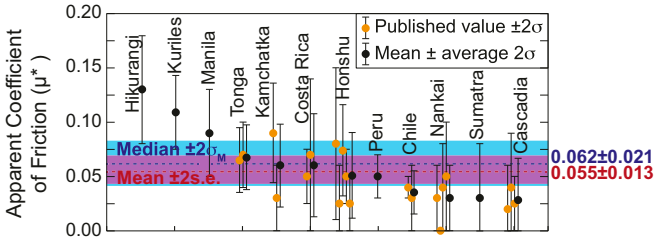

Fig. 2. Published values of μ* (*SI Appendix*), with mean ± 2 SE (blue band) and median ± 2_{SM} (red band) as calculated in this study.

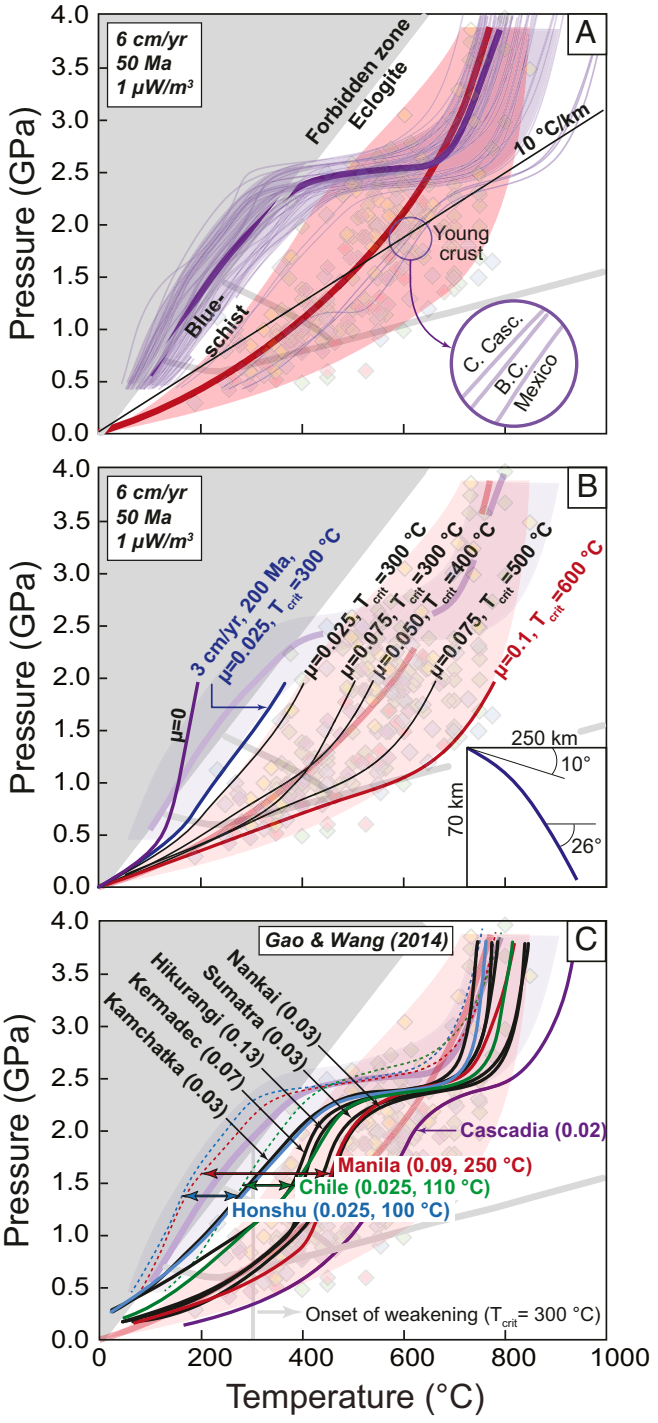

Fig. 3. (*A*) Data and models of slab-top geotherms. Pink region and curve are from PD15 (16); blue region bounds "normal" slab-top geotherms (11); blue curve is median slab-top geotherm (11) Gray lines show boundaries on metamorphic facies and on the forbidden zone (17). (*B*) Analytical models. Some sets of parameters could explain moderate- to low-temperature data equally well, e.g., high-μ plus low-T_{Crit}, low-μ plus high-T_{Crit}, etc.) Models with typical values of shear heating reported in the literature and based on global heat flow (Figs. 1 and 2) reproduce the PD15 geotherm. (*C*) Numerical models (34) with shear heating (solid lines). Dashed lines and double arrows show comparison with three similarly (but not identically) parameterized numerical models in which shear heating was excluded (11).

Thermal Models. Thermal models generally fall between two endmember types. Kinematic models fix subduction geometries, subduction rates, and rock thermal properties (e.g., refs. 19, 21, and 29). Dynamic models specify these same properties plus rock rheology, and allow the system to evolve in response to rock deformation and topographic changes (e.g., see review of ref. 30). Hybrid models typically specify geometries but include rock rheology to produce corner flow (mantle convection forced by traction along the subduction interface; e.g., see refs. 26, 27, and 31). Endmember kinematic models are simple, and the sensitivity to an input parameter is easily evaluated, but they do not model corner flow, which can increase temperatures at depths of 50–60 km by ~50 °C (32). Dynamic models arguably provide more realistic assessment of subduction zone processes, but numerous and highly variable input parameters complicate isolation of key factors to explain observations.

In this study, we use analytical models because they elucidate key parameters more simply than other types of models, especially the effects of shear heating. In that sense, they parallel earlier studies (13, 21, 24), but we compare them to more comprehensive datasets and consider combinations of parameters more representative of subduction zones (11). Thus, while our models do not supersede previous studies, they provide more focused examination of likely parameters in the context of quantitative data that have been compiled subsequently. We particularly emphasize that although many thermal models include shear heating (e.g., refs. 13, 21, 24, 26, and 33–36), many recent calculations of mineralogy, petrology, and geochemistry (2, 4, 9, 37) are either directly based on models that do not include shear heating or reference frictionless models as prima facie standards. If shear heating is important, as we argue (and as have several modelers), a large fraction of published geochemical and petrologic interpretations ranging from metamorphism and fluid release to arc volcanism must be reevaluated. Compilations of modern geophysical and geometric data (11), heat flow measurements (refs. 38 and 39 and Fig. 1), and the PD15 dataset afford the opportunity to reassess model accuracy with its implications for petrology, geophysics, and geochemistry.

Metamorphic Rock Density. Seminal calculations of rock density relevant to subduction zones (14, 18) were based on P–T fields corresponding with metamorphic facies, assuming an idealized chemical system or distribution of rocks across different P–T fields. These calculations do not account for continuous changes in mineral assemblage and mineral chemistry, but they do identify the most important shifts in density associated with (nearly) discontinuous reactions. In general, for a specified pressure, metamorphosed basalt is denser at higher temperatures, while hydrated peridotite shows a dramatic increase in density (~0.25 g/cm^3) at ~500 °C (14).

Rock Strength. Rock strength depends most on the weakest interconnected minerals. Rock mechanics measurements on weak sheet silicates ranging from talc to serpentine (40) extrapolated to geologic strain rates imply coefficients of friction (μ) ≥ 0.10 at subduction zone temperatures. Shear weakening can occur at seismic slip rates due to transient phenomena, although coefficients of friction are still typically ≥0.15 (41). Thermal weakening of rocks ultimately limits their ability to fracture or sustain high shear stress, and occurs at different temperatures for different bulk compositions. Weakening of quartz-rich rocks is typically modeled as initiating at ~300 °C (24), and patterns of seismicity in (basaltic) oceanic crust imply a brittle-plastic transition of ~600 °C (42). We use these limits as minimum and maximum temperatures of potential weakening.

Results

Heat Flow. Our global compilation of normalized heat flow data for subduction zones (Fig. 1 and *SI Appendix*, Fig. S1) plotted against normalized distance shows the expected drop in heat flow

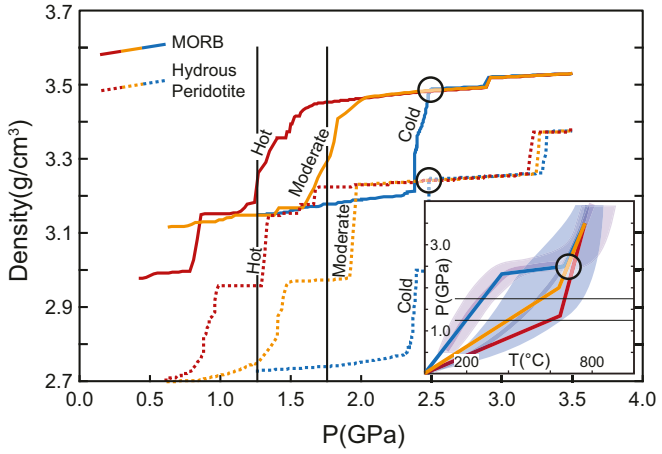

Fig. 4. Calculated density along representative hot, moderate, and cold P–T paths (*Inset*) for hydrated mid-ocean ridge basalt (MORB) and peridotite. Thin vertical lines bound regions of maximum differences between commonly accepted frictionless models and rock P–T conditions. Densities are always greatest for hot model and lowest for cold model.

close to the trench, then a rise toward the arc. For raw data (Fig. 1*A*) the rise is considerably steeper than for Cascadia (Fig. 1*B*) or for trench-length–normalized data (Fig. 1*C*). Cascadia shows high heat flow anomalies seaward of the trench associated with hydrothermal systems (e.g., ref. 43) and especially low normalized heat flow (<0.5) landward (Fig. 1*B*). Data that have been trench-length–normalized (Fig. 1*C*) show unusually low values close to the trench. Slabs and overriding plates seismically couple to 50–80-km depth (ref. 44; i.e., up to normalized distances ≥0.7 for an average subduction geometry), and viscously couple to drive mantle wedge convection deeper than ∼80-km depth (33). Relative to analytical models of slab-top geotherms, the magnitude of the heat flow minimum and rate of rise for the raw data imply an apparent coefficient of friction (μ^*) ≥ 0.1 (Fig. 1*A*). A similar comparison for Cascadia implies a lower coefficient of friction of ∼0.05 (Fig. 1*B*), but models are insensitive to μ^* (note close spacing of model curves) and sensitive to the assumed heat flux of the incoming plate and subduction geometry. Fully parameterized models (e.g., ref. 34) may provide better estimates of μ^* for Cascadia (Fig. 2). Trench-length–normalized data cannot be fit well for normalized distances of up to 0.2 but a μ^* value of ∼0.035–0.06 would fit most of the data for normalized distances up to 0.5. With the caveat that the analytical models are highly simplified, we take a value of ∼0.05 as best representing the data. Compilation of published coefficients of friction for specific subduction zones (see *SI Appendix* for data sources) implies similar ranges of 0.02–0.13 (Fig. 2), with mean and median values of 0.055 ± 0.013 (2 SE) and 0.062 ± 0.021 ($2\sigma_M$), respectively. Values of 0.05–0.06 for μ^* are higher than typically assumed in previous thermal models, but far lower than values for μ of 0.2–0.5 determined from deformation experiments of weak sheet silicates (40).

Models. Analytical models show that the slab-top geotherm is most sensitive to μ^*, slab angle, and temperature of thermal weakening (*SI Appendix*, Figs. S3 and S4) consistent with previous studies (21). Models that combine realistic bounds for these parameters have likely slab-top geotherms that span the PD15 dataset (Fig. 3 and *SI Appendix*, Figs. S3 and S4). In fact, a geotherm that closely parallels the PD15 slab-top geotherm results from using a value for μ^* of 0.05, comparable to estimates from global heat flow (Fig. 1*C*) and studies of specific subduction zones (Fig. 2); an average subduction rate and age of subducting plate as estimated from global compilations [6 cm/y, 50 Ma (11)]; a typical geometry (central Chile); and a moderate temperature of thermal weakening (400 °C; Fig. 3*A*).

Recent thermal models that include shear heating (34) predict slab-top geotherms that parallel ours for low pressures but steepen considerably at a temperature of ∼400 °C (Fig. 3*C*). Consequently, these geotherms overlap the lower-T and lower-P portion of the PD15 dataset, but fall toward the colder side of the distribution at higher pressures. This behavior reflects a relatively low temperature for the onset of thermal weakening of 300 °C. This temperature is the minimum bound that others have considered (24) (as do we: See *SI Appendix*, Fig. S4). Different numerical models that are parameterized differently, especially such that shear heating was included (34) vs. excluded (11), show quite different slab-top temperatures. Models that include shear heating show much closer correspondence with PD15, at least at low pressure and low temperature (Fig. 3*C*).

Rock Density. Density increases with pressure (and temperature; Fig. 4), with distinct step-ups as dehydration reactions are crossed. Rocks that follow higher-temperature P–T paths consistently show higher densities. The disparity is greatest at a pressure of ∼1.75 GPa (∼60-km depth), where the densities of high-temperature metabasalt and hydrated peridotite exceed those of their low-temperature counterparts by 0.25–0.5 g/cm^3. Disparities are evident between 1.25 and 1.75 GPa for cold/moderate- vs. hot P–T paths but disappear at ∼2.5 GPa where P–T paths converge.

Discussion

Heat Flow and Friction Are Relatively High. Previous regional studies (*SI Appendix*) and our compilation are congruent in demonstrating that heat flow in the forearc is higher than can be explained by $\mu^* \leq 0.02$. The negative heat flow anomaly close to the trench possibly reflects hydrothermal cooling of the oceanic plate (23, 45) rather than an absence of friction. Both the global datasets (Fig. 1*C*) and specific studies (Fig. 2) converge on average and median values for μ^* of 0.04–0.065, which exceed more typically assumed values of 0.0–0.03 (e.g., refs. 9–11, 31, and 33). Provisional values of average $\mu^* = 0.05 \pm 0.015$ and minimum $\mu^* = 0.03$ satisfy observations and may be preferred for future modeling, at least until more comprehensive analysis is undertaken that eliminates biases on a case-by-case basis. The disparity between coefficients of friction determined from natural data (low μ^*) vs. experiments (high μ) may reflect high pore fluid pressures or dynamic weakening at seismic slip rates, due to flash melting, pressurization of pore fluids, formation of weak silica gel, or loss of grain-to-grain contact (see summary of ref. 41).

Shear Heating Reconciles Thermal Models with Metamorphic P–T Conditions. The difference in predicted temperature between models that include shear heating (34) (Fig. 3) vs. those that omit shear heating (9–11) is especially striking: even the smallest proposed coefficient of friction (0.02–0.03) (34) raises slab-top temperatures by ≥100 °C at pressures of 1.5–2.0 GPa and permits predicted slab-top geotherms to intersect a substantial portion of the PD15 data set. Use of our preferred value for μ^* of 0.05 repositions average slab-top geotherms from near the boundary of the forbidden zone to the average PD15 geotherm (Fig. 3*A*). On a case-by-case basis, numerical models that include vs. exclude shear heating show temperature differences of 100–250 °C (Fig. 3*C*), although other modeling parameters besides μ^* also differ and could contribute to the difference. Overall, a broad range of friction coefficients inferred from forearc heat flow implies that a range of slab-top geotherms comparable to natural data are possible, and arguably likely. Many numerical models that predict metamorphic facies distributions have

assumed μ* values as low as 0.00–0.02 (e.g., refs. 9, 13, 24, 26–28, and 31), although values of 0.03–0.05 have also been considered (46, 47). A recent study (34) did not assume a value of μ*, rather derived values over a range of subduction zones based on heat flow, but did not evaluate the implications for metamorphic conditions. While many of these studies have presented P–T distributions of slab-top geotherms, comparison with the rock record has been lacking. Fig. 3 represents a comparison between quantitative thermobarometric P–T conditions and models that include μ* over a range of values consistent with heat flow. Overall, models that include shear heating (Fig. 3 *A* and *B*) are much more consistent with the PD15 dataset. Inasmuch as shear heating is inevitable, this correspondence implies that petrologic data are not restricted to subduction of anomalously young lithosphere or to subduction initiation (10). Consequently, we recommend that calculations that require a typical slab-top geotherm use the average PD15 geotherm (T in °C)

$$\mathrm{P\ (GPa)} = 1.533\times10^{-3}\cdot \mathrm{T} \ + \ 5.07\times10^{-9}\cdot \mathrm{T}^3. \qquad [1]$$

In that context, the ±2σ bounds on the PD15 distribution (Fig. 3) reflect the range of expected subduction conditions. Data and geotherms outside those bounds may be viewed as unusual. In reference to disparities between PD15 and many thermal models, other sources of heat along the subduction interface are possible, for example heat advection and production via rock convection, fluid flow, and hydration reactions (see summary of ref. 16). Nonetheless, shear heating provides a simple explanation to reconcile differences between rock P–T conditions and thermal model predictions.

Exhumation of Subduction Zone Rocks. Recent models have been used to argue that buoyancy favors rock exhumation from subduction of extremely young crust or subduction initiation (10), i.e., hot subduction settings. However, from a petrologic perspective (14), higher temperatures enhance densification compared with lower temperatures. All slabs undergo hydrothermal alteration at the ridge axis, so arguably they should all have similar water content upon subduction. If so, hotter subduction zones should be less amenable to buoyant exhumation because they densify through eclogitization and deserpentinization at a lower pressure (Fig. 4). For example, in a hot subduction zone, at a depth of ∼60 km (1.75 GPa), metabasalt and hydrated metaperidotite are ∼10% and ∼15% denser, respectively, than in a cold subduction zone. Reaction kinetics can also retard eclogitization of drier plutonic rocks (e.g., ref. 48), but insofar as higher temperatures speed kinetics, transformation of anhydrous oceanic crust to eclogite should occur at shallower levels in hot subduction zones than in cold subduction zones. That is, hotter subduction zones may well have denser rocks throughout the oceanic crust—not only in hydrated metabasalts and metaperidotite but also in anhydrous gabbros—and their rocks may be less amenable to exhumation than in cold subduction zones.

Implications for Rock Strength and Temperatures of Thermal Weakening. A temperature of 300 °C marks a transition from brittle to plastic deformation behavior in quartz at low geologic strain rates [10^{-15} s^{-1} (49)], and is commonly assumed to represent conditions of thermal weakening. Similarly, field studies of quartz microstructures in mylonites often return low differential stresses of only 10–20 MPa (e.g., ref. 50). For a typical subduction zone geotherm of ∼10 °C/km and a coefficient of friction of 0.05, these values imply a transition from brittle to ductile behavior at depths of 20–40 km (∼1.0 GPa; see ref. 50), which is too shallow to explain the large number of rock P–T conditions at 1.5–2.0 GPa and 500–600 °C. In part these discrepancies may reflect strain rate. For a subduction rate of 6 cm/y distributed over a 1-km-thick shear zone, the strain rate is very high, $\sim 2\times10^{-12}\cdot s^{-1}$. At high strain rate, rocks can sustain greater shear stresses and produce more heat, although increasing water fugacity at higher pressures mitigates this effect. Regardless, to control the strength of the subduction interface, weak quartzites would have to occur as continuous sheets. Bending-related horst-and-graben formation likely disrupts the thin sedimentary carapace of the oceanic crust, while trench turbidite infill is clay-rich and discontinuous both spatially and temporally. Both factors make strength continuity unlikely.

Implications for Earthquakes and Arc Volcanism. Seismic and geodetic networks define the seismogenic zone as a region where interplate locking promotes elastic energy buildup extending to 40–60-km depth (7). This region grades into the interplate fault segment that moves by slow-slip phenomena for 20–40-km down-dip (51). Intermediate-depth intraslab seismicity extends another 200–300-km down-dip. Thermally controlled processes possibly trigger the form of failure (5–7), but the uncertainties described above have hindered definitive identification of rocks containing the mineral assemblages and (micro)structures required to identify the metamorphic facies, rheological properties, and fault mechanics of each of the different-depth slip phenomena. In light of revised μ*, generally hotter models should be considered to identify the deformation phenomena at play.

Although we view the thermal structure of subduction zones above 80-km depth as considerably hotter than many recent models, inferences of the mineralogical drivers of arc volcanism remain robust. Because full mantle wedge convection at depths ≥80 km (≥2.5 GPa) controls heat budgets, the slab-top thermal structure of the deeper portions of subduction systems in these recent models (10, 11, 31) should converge with the P–T conditions of rocks that record pressures of >2.5 GPa (16), as observed (Fig. 3). Because it is the deep, not shallow thermal structure that defines hydrous mineral stability at depths ≥80 km, dehydration of hydrous peridotites still could catalyze arc formation (4).

Methods

We obtained heat flow data (39) from W. Gosnold and limited data to within 350 km of subduction zone plate boundaries (52). We added data from Tonga/Kermadec (53), which were otherwise missing. We did not intend to seek out every heat flow measurement, but rather to compile sufficient data to gain insights into heat flow distributions. We eliminated ∼1,000 measurements that were from extensional zones, and separated Cascadia (∼4,000 measurements) from other subduction zones (∼5,000 measurements). We accounted for the effect of plate age (11) on heat flow by normalizing heat flow data to the expected heat flow for the age of the subducting plate (25). We did not account for convergence rate because modeling shows that it does not have a major effect on thermal structure (*SI Appendix*, Figs. S3 and S4). Distances were normalized for each datum by ratioing the distance perpendicular to the trench with the arc–trench distance (11). In this scheme, a heat flow value of 1.0 represents the expected heat flow for the age of the subducting plate, a distance of 0.0 represents the position of the trench, and a distance of +1.0 represents the position of the arc.

Data are scattered (Fig. 1), so we binned data and used medians. Errors are two times the median absolute deviation divided by the square root of the number of data in the bin. To address data bias, we randomly subsampled data between the arc and the trench (normalized distances between 0.02 and 1.0) such that the number of data points was proportional to the length of the subduction zone trench. Our choice of a lower bound of 0.02 reflects slight disparities between the tabulated positions of the plate boundary (52) vs. the topographically identified position of the trench. Subsampling allowed us to include observations from both highly- (e.g., Cascadia) and sparsely- (e.g., Andes) sampled subduction zones.

Because of its flexibility, we used an analytical model that includes shear heating to model the thermal structure of the subduction interface (Fig. 3 and refs. 19 and 20). We calculated slab-top temperatures to depths of 66 km because it conveniently corresponds with a pressure of ∼2.0 GPa, and because corner flow significantly impacts thermal structure at this level and deeper. The analytical model requires specifying numerous subduction

parameters as described in *SI Appendix*, most importantly slab geometry, coefficient of friction, and temperature of thermal weakening. Slab geometry was taken from central Chile, which has an intermediate geometry down to depths of ∼100 km of the subduction zones considered in this study (*SI Appendix*, Fig. S2). For modeling, we assumed coefficients of friction from 0 (frictionless) to 0.1. The upper bound is within error of the highest values that data suggest (Fig. 2), and suffices to illustrate the impact of coefficients of friction on thermal structure. Temperatures of thermal weakening were assumed to range from 300 to 600 °C (24, 42). The effect of shear zone thickness on slab-top temperatures was derived analytically (*SI Appendix*). A shear zone thickness of 500 m to 5 km impacts calculated temperatures by a maximum of 0.6–6 °C, respectively.

Rock densities were calculated using standard thermodynamic models applied to bulk rock compositions characteristic of peridotite and mid-ocean ridge basalt (see *SI Appendix* for methods and references). We assume that any fluid produced escapes the rock. Solution models and density output are provided in *SI Appendix*. Modeled P–T paths are simplified representations of cold, intermediate, and hot slab-top geotherms (Fig. 4, *Inset*).

ACKNOWLEDGMENTS. We thank P. Molnar and S. Roecker for comments prior to submission, W. Gosnold and X. Gao for providing the global heat flow database and the slab-top geotherms from numerical models, L. Spaete for help parsing the global heat flow database, and P. Kelemen, T. Gerya, and four anonymous reviewers whose incisive comments helped improve the manuscript substantially. Support was provided by NSF Grants EAR1419865 and OISE1545903 (to M.J.K.), EAR1447468 and EAR1750674 (to F.S.S.), and the Spanish Ministry of Science under "Acción de Programación Conjunta Internacional" Grant PCIN-2015-053 (to C.R.R.).

1. Bebout GE, Penniston-Dorland SC (2016) Fluid and mass transfer at subduction interfaces—The field metamorphic record. *Lithos* 240–243:228–258.
2. Kelemen PB, Manning CE (2015) Reevaluating carbon fluxes in subduction zones, what goes down, mostly comes up. *Proc Natl Acad Sci USA* 112:E3997–E4006.
3. Manning C (2004) The chemistry of subduction-zone fluids. *Earth Planet Sci Lett* 223: 1–16.
4. Grove TL, Till CB, Krawczynski MJ (2012) The role of H2O in subduction zone magmatism. *Annu Rev Earth Planet Sci* 40:413–439.
5. Hacker BR, Peacock SM, Abers GA, Holloway SD (2003) Subduction factory 2. Are intermediate-depth earthquakes in subducting slabs linked to metamorphic, dehydration reactions? *J Geophys Res Solid Earth*, 10.1029/2001jb001129.
6. Hyndman RD (2013) Downdip landward limit of Cascadia great earthquake rupture. *J Geophys Res Solid Earth* 118:5530–5549.
7. Wang K, Tréhu AM (2016) Invited review paper: Some outstanding issues in the study of great megathrust earthquakes—The Cascadia example. *J Geodyn* 98:1–18.
8. Hacker BR (2008) H2O subduction beyond arcs. *Geochem Geophys Geosyst*, 10.1029/2007gc001707.
9. van Keken PE, Hacker BR, Syracuse EM, Abers GA (2011) Subduction factory: 4. Depth-dependent flux of H2O from subducting slabs worldwide. *J Geophys Res*, 10.1029/2010jb007922.
10. Abers GA, van Keken PE, Hacker BR (2017) The cold and relatively dry nature of mantle forearcs in subduction zones. *Nat Geosci* 10:333–337.
11. Syracuse EM, van Keken PE, Abers GA (2010) The global range of subduction zone thermal models. *Phys Earth Planet Inter* 183:73–90.
12. van den Beukel J, Wortel R (1987) Temperatures and shear stresses in the upper part of a subduction zone. *Geophys Res Lett* 14:1057–1060.
13. Peacock SM (1993) The importance of blueschist -> eclogite dehydration reactions in subducting oceanic crust. *Geol Soc Am Bull* 105:684–694.
14. Hacker BR (1996) Eclogite formation and the rheology, buoyancy, seismicity, and H2O content of oceanic crust. *Geophys Monogr* 96:337–346.
15. Hacker BR (2006) Pressures and temperatures of ultrahigh-pressure metamorphism: Implications for UHP tectonics and H2O in subducting slabs. *Int Geol Rev* 48: 1053–1066.
16. Penniston-Dorland SC, Kohn MJ, Manning CE (2015) The global range of subduction zone thermal structures from exhumed blueschists and eclogites: Rocks are hotter than models. *Earth Planet Sci Lett* 428:243–254.
17. Liou JG, Hacker BR, Zhang RY (2000) Into the forbidden zone. *Science* 287:1215–1216.
18. Hacker BR, Abers GA, Peacock SM (2003) Subduction factory 1. Theoretical mineralogy, densities, seismic wave speeds, and H2O contents. *J Geophys Res Solid Earth*, 10.1029/2001jb001127.
19. Molnar P, England PC (1990) Temperatures, heat flux, and frictional stress near major thrust faults. *J Geophys Res* 95:4833–4856.
20. Tichelaar BW, Ruff LJ (1993) Depth of seismic coupling along subduction zones. *J Geophys Res* 98:2017–2037.
21. Dumitru TA (1991) Effects of subduction parameters on geothermal gradients in forearcs, with an application to Franciscan subduction in California. *J Geophys Res* 96: 621–641.
22. Rotman HMM, Spinelli GA (2013) Global analysis of the effect of fluid flow on subduction zone temperatures. *Geochem Geophys Geosyst* 14:3268–3281.
23. Spinelli GA, Wang K (2009) Links between fluid circulation, temperature, and metamorphism in subducting slabs. *Geophys Res Lett*, 10.1029/2009gl038706.
24. Peacock SM, Rushmer T, Thompson AB (1994) Partial melting of subducting oceanic crust. *Earth Planet Sci Lett* 121:227–244.
25. Stein CA (2003) Heat flow and flexure at subduction zones. *Geophys Res Lett*, 10.1029/2003gl018478.
26. Peacock SM (1996) Thermal and petrologic structure of subduction zones. *Geophys Monogr* 96:119–133.
27. Peacock SM (2003) Thermal structure and metamorphic evolution of subducting slabs. Geophysical Monograph (American Geophysical Union, Washington, DC), Vol 138, pp 7–22.
28. Rosas JC, Currie CA, Harris RN, He J (2016) Effect of hydrothermal circulation on slab dehydration for the subduction zone of Costa Rica and Nicaragua. *Phys Earth Planet Inter* 255:66–79.
29. Peacock SM (1987) Creation and preservation of subduction-related inverted metamorphic gradients. *J Geophys Res* 92B:12763–12781.
30. Gerya T (2011) Future directions in subduction modeling. *J Geodyn* 52:344–378.
31. van Keken PE, Kiefer B, Peacock SM (2002) High-resolution models of subduction zones: Implications for mineral dehydration reactions and the transport of water into the deep mantle. *Geochem Geophys Geosyst*, 10.1029/2001gc000256.
32. Wada I, Wang K, He J, Hyndman RD (2008) Weakening of the subduction interface and its effects on surface heat flow, slab dehydration, and mantle wedge serpentinization. *J Geophys Res* 113:B04402.
33. Wada I, Wang K (2009) Common depth of slab-mantle decoupling: Reconciling diversity and uniformity of subduction zones. *Geochem Geophys Geosyst*, 10.1029/2009gc002570.
34. Gao X, Wang K (2014) Strength of stick-slip and creeping subduction megathrusts from heat flow observations. *Science* 345:1038–1041.
35. Rotman HMM, Spinelli GA (2014) Remarkably consistent thermal state of the south central Chile subduction zone from 36°S to 45°S. *J Geophys Res Solid Earth* 119: 3503–3516.
36. Harris RN, et al. (2010) Thermal regime of the Costa Rican convergent margin: 2. Thermal models of the shallow Middle America subduction zone offshore Costa Rica. *Geochem Geophys Geosyst*, 10.1029/2010gc003273.
37. Spandler C, Pirard C (2013) Element recycling from subducting slabs to arc crust: A review. *Lithos* 170:208–223.
38. Hasterok D, Chapman DS, Davis EE (2011) Oceanic heat flow: Implications for global heat loss. *Earth Planet Sci Lett* 311:386–395.
39. Gosnold W (2010) The global heat flow database. Available at https://redevelop-engineering.und.edu/academics/geology-and-geological/globe-heat-flow-database/data.html. Accessed April 2, 2018.
40. Moore DE, Lockner DA (2007) Comparative deformation behavior of minerals in serpentinized ultramafic rock: Application to the slab-mantle interface in subduction zones. *Int Geol Rev* 49:401–415.
41. Tullis TE (2015) Mechanisms for friction of rock at earthquake slip rates A2. *Treatise on Geophysics*, ed Schubert G (Elsevier, Oxford), 2nd Ed, pp 139–159.
42. Chen W-P, Molnar P (1983) The depth distribution of intracontinental and intraplate earthquakes and its implications for the thermal and mechanical properties of the lithosphere. *J Geophys Res* 88:4183–4214.
43. Davis EE, Hyndman RD, Villinger H (1990) Rates of fluid expulsion across the northern Cascadia accretionary prism: Constraints from new heat flow and multichannel seismic reflection data. *J Geophys Res* 95:8869–8889.
44. Hayes GP, Wald DJ, Johnson RL (2012) Slab1.0: A three-dimensional model of global subduction zone geometries. *J Geophys Res Solid Earth*, 10.1029/2011jb008524.
45. Harris RN, Spinelli GA, Fisher AT (2017) Hydrothermal circulation and the thermal structure of shallow subduction zones. *Geosphere* 13:1425–1444.
46. Harris RN, Wang K (2002) Thermal models of the Middle America Trench at the Nicoya Peninsula, Costa Rica. *Geophys Res Lett*, 10.1029/2002gl015406.
47. Perry M, Spinelli GA, Wada I, He J (2016) Modeled temperatures and fluid source distributions for the Mexican subduction zone: Effects of hydrothermal circulation and implications for plate boundary seismic processes. *Geochem Geophys Geosyst* 17: 550–570.
48. Austrheim H, Griffin WL (1985) Shear deformation and eclogite formation within granulite-facies anorthosites of the Bergen Arcs, Western Norway. *Chem Geol* 50: 267–281.
49. Hirth G, Teyssier C, Dunlap WJ (2001) An evaluation of quartzite flow laws based on comparisons between experimentally and naturally deformed rocks. *Int J Earth Sci* 90: 77–87.
50. Behr WM, Platt JP (2014) Brittle faults are weak, yet the ductile middle crust is strong: Implications for lithospheric mechanics. *Geophys Res Lett* 41:8067–8075.
51. Peng Z, Gomberg J (2010) An integrated perspective of the continuum between earthquakes and slow-slip phenomena. *Nat Geosci* 3:599–607.
52. Bird P (2003) An updated digital model of plate boundaries. *Geochem Geophys Geosyst*, 10.1029/2001gc000252.
53. Von Herzen R, et al. (2001) A constraint on the shear stress at the Pacific-Australian plate boundary from heat flow and seismicity at the Kermadec forearc. *J Geophys Res Solid Earth* 106:6817–6833.